

Consistent inclusion of triple substitutions within a coupled cluster based static quantum embedding theory

Avijit Shee,¹ Fabian M. Faulstich,² K. Birgitta Whaley,^{1,3} Lin Lin,^{4,5} and Martin Head-Gordon¹

¹*Department of Chemistry, University of California, Berkeley, CA 94720, USA*

²*Department of Mathematics, Rensselaer Polytechnic Institute, Troy, NY 12180, USA*

³*Berkeley Center for Quantum Information and Computation, Berkeley, CA 94720, USA*

⁴*Department of Mathematics, University of California, Berkeley, CA 94720, USA*

⁵*Applied Mathematics and Computational Research Division,
Lawrence Berkeley National Laboratory, Berkeley, CA 94720, USA*

(Dated: February 16, 2026)

We have previously proposed the MPCC static embedding framework for quantum chemistry that self-consistently couples a high-level coupled cluster (CC) treatment of the fragment (active region) with a lower level, Møller-Plesset perturbation treatment of the environment. Our initial implementation was limited to single and double (SD) substitutions, with CCSD for the fragment, and first-order perturbative SD amplitudes for the environment. Here, we extend the MPCC embedding treatment to triple substitutions, which is essential for achieving chemical accuracy in energy differences. To this end, we employ a CCSDT solver for the fragment subsystem. For the environment subsystem, we construct a perturbative estimate of the triples amplitudes, explicitly accounting for feedback from all fragment amplitudes. The resulting approach is denoted MPCCSDT(pt). We further introduce a more complete formulation in which feedback from the environment amplitudes to the fragment amplitudes is also included. This scheme involves an iterative treatment of the environment triples amplitudes and is denoted MPCCSDT(it). In addition, we assess the accuracy of the previously proposed low-level method by introducing a modified low-level approach that incorporates a lowest-order treatment of selected long-range effects, including spin fluctuations and charge polarization. All resulting approaches may be viewed as post-CCSD(T) methods. We therefore consider test cases for which CCSD(T) exhibits substantial deviations from CCSDT. These include (i) single- and triple-bond stretching in F_2 and N_2 , (ii) bond dissociation energies of selected molecules from the W4-11 dataset, and (iii) total atomization energies of transition metal hydrides. Our results demonstrate that inclusion of triples amplitudes at the fragment level alone is insufficient; a perturbative treatment of the environment triples amplitudes is required. For many energy-difference applications, feedback from the environment triples amplitudes to the fragment amplitudes, is not essential, but it does play a role in the very challenging CoH and FeH molecules. A very interesting finding from our study is that in some challenging cases we need an improved (second-order) perturbative method for the SD amplitudes, going beyond the first-order one used in our earlier work. Considering both cost and accuracy, the MP2CCSDT(pt) model is the most promising for future applications among the candidates considered here.

I. INTRODUCTION

Wavefunction-based approaches to quantum chemistry are most commonly based on a single determinant reference, such as the mean-field Hartree-Fock wavefunction. The electron correlation energy [1], $E_{\text{corr}} = E - E_{\text{HF}}$, is only $\sim 1\%$ of the total energy, but is critical for calculating reliable energy differences because E_{corr} changes in most chemical transformations (albeit with important exceptions such as isodesmic reactions [2] and the like) as bonds are made and broken. Treating electron correlation at just the level of singles and doubles (SD) is also not adequate to achieve quantitative accuracy in energy differences, as has been known since the first implementations of triples (T) as part of fourth order Møller-Plesset (MP) perturbation theory[3].

Coupled cluster (CC) [4, 5] theory has become the predominant approach to electron correlation, as truncation of the amplitudes at any level of excitation (CCSD, CCSDT, etc) leaves polynomial-scaling equations for the amplitudes and guarantees size-consistent energies. The

comparative compute costs and storage requirements for low-order CC theory, as well as for low-order MP theory are summarized in Table I. Based on the very large gap in storage and compute requirements between CCSD and CCSDT, the perturbative treatment of triples, CCSD(T) [6], has become the most popular way of including the triples. For most cases where the HF reference is a qualitatively good starting point, CCSD(T) is very successful, to the extent that it has become known as the “gold standard” of quantum chemistry. Furthermore, CCSD(T) has storage requirements that do not exceed CCSD, and its compute effort scales as non-iterative $\mathcal{O}(O^3V^4)$ versus iterative $\mathcal{O}(O^3V^5)$ for CCSDT.

However, there are some regimes in which CCSD(T) demonstrably fails. Most clear-cut are the cases where triple substitutions are not a perturbative correction to the wavefunction, as assumed in CCSD(T), but are instead quite large. Such cases are typical of molecules or systems that exhibit strong electron correlations, such as partially recoupled unpaired electrons. For example, in Cr_2 , 2 ^{7}Cr atoms are recoupled to $^{1}Cr_2$, but

Method	Iterative		Perturbative	
	Compute	Memory	Compute	Memory
MP2	-	-	$\mathcal{O}(O^2V^2X)$	$\mathcal{O}(ONX)$
MP3	-	-	$\mathcal{O}(O^2V^4X)$	$\mathcal{O}(ONX)$
CCSD	$\mathcal{O}(O^2V^4)$	$\mathcal{O}(O^2V^2)$	-	-
CCSD(T)	$\mathcal{O}(O^2V^4)$	$\mathcal{O}(O^2V^2)$	$\mathcal{O}(O^3V^4)$	-
CCSDT	$\mathcal{O}(O^3V^5)$	$\mathcal{O}(O^3V^3)$	$\mathcal{O}(O^3V^4)$	-

TABLE I. Compute and memory scaling requirements with problem size for conventional coupled cluster theory through triple substitutions and low-order Møller-Plesset perturbation theory. O, V, X denote the size of the occupied space, the virtual space, and the auxiliary basis set, respectively.

the binding energy of 137 kJ/mol is weaker than a typical single bond rather than a hexuple bond[7]. Other transition metal diatomics with partial spin recoupling are also very challenging for CCSD(T) [8]. Metalloenzymes with multiple metal centers are also considered to be strongly correlated molecules. Another class of failure of CCSD(T) is when the HF orbitals exhibit significant symmetry breaking (such as spin contamination) which is not properly recovered in its triples correction. If the symmetry-breaking is artificial (rather than a consequence of strong correlation) then use of alternative orbitals such as from Kohn-Sham density functional theory (DFT) can be helpful [9, 10]. Finally, even in the intermolecular interactions between large π -electron molecules such as the so-called Buckycatcher complex, there is unresolved debate over whether CCSD(T) is adequate or not [11–13].

The strategy used in methods like CCSD(T) and its higher order analogs such as CCSDT(Q) [14] is an all-or-nothing choice between which amplitudes are treated self-consistently by CC theory, and which are approximated perturbatively. In other words, in CCSD(T), the SD amplitudes are iterated, and the T amplitudes are treated perturbatively. Indeed in CCSD and CCSDT all amplitudes are iterated and none are treated perturbatively. However, not all amplitudes at a given level of substitution are equally significant. Typically only a small fraction are large (corresponding to excitations within the valence space), while others that involve the very high energy price of promotions in the principal quantum number to access higher virtual levels are typically small. Therefore, it is reasonable to seek methods that do not make the “all or none” decision for a given class of amplitudes, but instead partition them into a “primary set” that should be iterated, and a “secondary set” that can be perturbatively approximated.

To make such an approach well-defined, rather than depending upon some arbitrary threshold for switching between primary and secondary, it is best to introduce a well-defined partition of the 1-particle orbitals into a primary and secondary set. The primary set could be a small basis (even a valence minimal basis) and the secondary set could be the missing orbitals (core and higher virtuals) necessary to comprise the target extended basis. This is reminiscent of dual basis methods for HF and DFT calculations[15–18], but carries the concept

much further. In fact it is a particular type of quantum mechanical/quantum mechanical (QM/QM) embedding theory, where the question is how best to couple the primary amplitudes (that involve substitutions *entirely within* the primary orbital set) and the secondary amplitudes (that involve substitutions that at least *partly* involve the secondary orbital set).

A rigorous (QM/QM) embedding framework was first formulated in the context of Green’s function-based many-body theory by Georges *et al.* [19, 20] in their dynamical mean field theory (DMFT) work. The DMFT formulation utilizes frequency-dependent/dynamical quantities such as Green’s functions and the self-energy for the embedding construction. However, if static observables, such as total energy, dipole moment, spectroscopic parameters, etc. are the target quantities, a simpler static formulation is also possible. Density matrix embedding theory (DMET)[21, 22] is a prominent example of this direction.

A crucial component of the embedding methods is the choice of a high-accuracy solver for the fragment problem. For practical molecular and materials applications, the dimensionality of the fragment is typically not very small; therefore to avoid the exponential scaling of full configuration interaction solvers,[23] CC theory is considered to be a viable, systematically improvable alternative with polynomial cost. It has been explored both in the context of DMFT [24, 25], its variants [26] and DMET [27]. However, many of those approaches suffer from the lack of systematic accuracy and/or have insufficient theoretical robustness.

A potentially well-defined alternative is to concentrate on coupling (high level) many-body CC with (lower level) perturbative methods in static embedding theory. Seminal efforts to combine CCSD (high level) and MP2 (low level) were the methods developed by Nooijen [28] and Sherrill [29, 30], which demonstrated the importance of self-consistent coupling of the MP and CC amplitudes. In turn these methods relied on earlier work[31, 32] that partitioned the cluster operator into internal and external components. Our recent work built on these and other developments[33–36] to yield a self-consistent coupling between MP2 and CCSD (called MPCCSD) within a general MPCC wave function based static embedding theory[37]. The MPCC approach is designed from the outset to enable well-defined, black-box partitioning of

the system into fragment and environment amplitudes, based on an active orbital window. Alternatively spatial locality can additionally be used to consider fragments that are local to just an active region.

In this work, the same MPCC framework will be utilized to try to achieve the aforementioned goal of achieving quantitative accuracy for problems where CCSD(T) typically fails. In order to achieve this goal we have considered the iterative CCSDT method[38] as a high-level fragment solver. The challenge is to design and assess one or more perturbation treatments that can describe the environment. The simplest option is to include only singles and doubles amplitudes in the environment, but one can also (and indeed we will show that one must also) include environment triples amplitudes.

II. THEORY

A. Brief recap of the MPCC method

In the MP-CC approach, we partition the total orbital space into a set of (active) fragment (F) orbitals and a set of (inactive) environment (E) orbitals. The fragment orbitals describe the chemically relevant region requiring higher accuracy, spanning only a few atoms, localized bonds, or a chemically relevant subspace of the full basis set. The environment orbitals, on the other hand, will describe the remainder of the system. A valid partition of a given orbital set $\{\phi_i\}_{i=1}^K$ is specified by disjoint index sets that assign each occupied and virtual orbital to either the fragment or the environment. Assuming an N electron system, the occupied space is,

$$O = O_E \cup O_F, \quad (1)$$

where $O = \{\phi_i : 1 \leq i \leq N\}$ and

$$O_E = \{\phi_i : i \in \mathcal{I}_{\text{occ}}^E\}, \quad O_F = \{\phi_i : i \in \mathcal{I}_{\text{occ}}^F\}, \quad (2)$$

with $\mathcal{I}_{\text{occ}}^E \cap \mathcal{I}_{\text{occ}}^F = \emptyset$ and $\mathcal{I}_{\text{occ}}^E \cup \mathcal{I}_{\text{occ}}^F = \llbracket N \rrbracket = \{1, \dots, N\}$. The virtual space is partitioned similarly:

$$V = V_E \cup V_F, \quad V = \{\phi_i : i > N\}, \quad (3)$$

where $V = \{\phi_i : N < i < K\}$ and

$$V_E = \{\phi_i : i \in \mathcal{I}_{\text{vir}}^E\}, \quad V_F = \{\phi_i : i \in \mathcal{I}_{\text{vir}}^F\} \quad (4)$$

with $\mathcal{I}_{\text{vir}}^E \cap \mathcal{I}_{\text{vir}}^F = \emptyset$ and $\mathcal{I}_{\text{vir}}^E \cup \mathcal{I}_{\text{vir}}^F = \llbracket K \rrbracket \setminus \llbracket N \rrbracket$. We denote the number of fragment and environment orbitals by $N_F = |\mathcal{I}_{\text{occ}}^F| + |\mathcal{I}_{\text{vir}}^F|$ and $N_E = |\mathcal{I}_{\text{occ}}^E| + |\mathcal{I}_{\text{vir}}^E|$, respectively. We slightly abuse the notation by using O and V to denote both the sets of occupied and virtual orbitals, respectively, and their cardinalities. The intended meaning should be clear from the context.

We will use the indices i, j, k, l, \dots for the orbitals in the occupied space (O) and a, b, c, d, \dots for the orbitals in the virtual space (V). For orbitals in the fragment occupied

space (O_F) we use I, J, K, L , and for the fragment virtual space (V_F) we use A, B, C, D indices.

We note that the choice of basis to construct the fragment space plays a vital role in obtaining the desired accuracy with this method, similar to the other embedding approaches. In our previous work [37], we have utilized the active valence active space [39] (AVAS) scheme to construct this space, as it provides an automatic approach. Within the AVAS scheme, we aim to isolate a set of orbitals of interest (such as d-orbitals of a transition metal) from the full set of orbitals of a specific problem. Typically, a minimal atomic orbital basis (MINAO) is chosen to represent the region of interest, as it closely aligns with the idea of chemically relevant bonding and antibonding orbitals in the valence region. On the other hand, for the full calculation, we can (and should) choose a larger atomic orbital basis set. A special characteristic of the AVAS scheme is that higher angular momentum atomic orbitals can be trivially added to the active space by choosing a slightly larger basis set than the minimal one. This feature allows us to capture the strongest dynamical correlations within the active space and also provides a means to increase the active space size systematically.

Once a valid partition is made, we employ an exponential wavefunction parametrization,

$$|\Psi\rangle = e^T |\Phi_0\rangle, \quad T = \sum_{n \geq 1} T_n, \quad (5)$$

with

$$\begin{aligned} T_n &= \frac{1}{(n!)^2} \sum_{i_1 \dots i_n} \sum_{a_1 \dots a_n} t_{i_1 \dots i_n}^{a_1 \dots a_n} a_{a_1}^\dagger \dots a_{a_n}^\dagger a_{i_n} \dots a_{i_1} \\ &= \sum_{i_1 \dots i_n} \sum_{a_1 \dots a_n} t_{i_1 \dots i_n}^{a_1 \dots a_n} X_{i_1 \dots i_n}^{a_1 \dots a_n}, \end{aligned} \quad (6)$$

where X are particle-hole excitation operators [4]. We define the fragment contribution at excitation rank n as the restriction to fragment indices, i.e.,

$$T_n^F = \frac{1}{(n!)^2} \sum_{\substack{i_1, \dots, i_n \in \mathcal{I}_{\text{occ}}^F \\ a_1, \dots, a_n \in \mathcal{I}_{\text{vir}}^F}} t_{i_1 \dots i_n}^{a_1 \dots a_n} X_{i_1 \dots i_n}^{a_1 \dots a_n}, \quad (7)$$

and the environment contribution as its complement, i.e.,

$$T_n^E = T_n - T_n^F. \quad (8)$$

Equivalently, $T^F = \sum_{n \geq 1} T_n^F$ and $T^E = T - T^F$. We denote by \mathbf{t}^F and \mathbf{t}^E the collections of amplitudes appearing in T^F and T^E , respectively. Note that T^F collects excitation operators that act *exclusively* within the fragment orbital subspace. In contrast, T^E comprises all remaining amplitudes, i.e., (i) “purely” environmental excitations involving only environment orbitals and (ii) “mixed” fragment-environment excitations. The mixed terms capture correlations that couple fragment and environment degrees of freedom, e.g., excitations from fragment occupied orbitals into environment virtual orbitals,

or simultaneous excitations involving occupied orbitals from both regions.

In the spirit of quantum embedding, we will compute the cluster operators T^F and T^E at different levels of accuracy. Specifically, we determine the fragment cluster operator T^F using the standard CC formalism (the high-level, HL, theory in quantum embedding parlance), while treating the environment cluster operator T^E at a perturbative level (the lower-level, LL, theory). Put differently, the similarity-transformed Hamiltonian that enters the CC projection equations is treated differently in the fragment and environment theories. For the fragment, we use the full similarity-transformed Hamiltonian, i.e.,

$$\bar{H}(\mathbf{t}^F; \mathbf{t}^E) = e^{-T^E - T^F} H e^{T^F + T^E}, \quad (9)$$

whereas for the environment, we employ a lower-order perturbative approximation, denoted $\tilde{H}(\mathbf{t}^E; \mathbf{t}^F)$. The latter is theoretically more involved; a detailed discussion of the low-level Hamiltonians proposed and investigated here follows below. In overview, the MP-CC approach leads to two sets of coupled projective equations

$$\langle \Phi_\mu^F | \bar{H}^F(\mathbf{t}^F; \mathbf{t}^E) | \Phi_0 \rangle = 0, \quad (10)$$

$$\langle \Phi_\mu^E | \tilde{H}^E(\mathbf{t}^E; \mathbf{t}^F) | \Phi_0 \rangle = 0, \quad (11)$$

where $|\Phi_\mu^F\rangle$ and $|\Phi_\mu^E\rangle$ denote excited Slater determinants in the fragment and environment space, respectively. These coupled residual equations can be obtained from the stationarity of the MP-CC Lagrangian,

$$\begin{aligned} \mathcal{L}(\mathbf{t}, \boldsymbol{\lambda}) = & \langle \Phi_0 | \bar{H} | \Phi_0 \rangle + \langle \Phi_0 | \Lambda^F \bar{H}^F(\mathbf{t}^F; \mathbf{t}^E) | \Phi_0 \rangle \\ & + \langle \Phi_0 | \Lambda^E \tilde{H}^E(\mathbf{t}^E; \mathbf{t}^F) | \Phi_0 \rangle, \end{aligned} \quad (12)$$

where $\Lambda^Y = \sum_{\mu \in Y} \lambda_\mu^Y X_\mu^Y$ for $Y \in \{F, E\}$, and the first term in the Lagrangian is the coupled cluster energy for the total system (fragment + environment); therefore the \bar{H} remained unlabeled.

We emphasize that both \bar{H}^F and \tilde{H}^E in Eqs. (10) and (11) depend on the full set of cluster amplitudes, i.e., \mathbf{t}_F and \mathbf{t}_E . However, when solving the fragment residual equations, \mathbf{t}_E is held fixed and \mathbf{t}_F is updated, whereas in solving the environment residual equations, \mathbf{t}_F is held fixed and \mathbf{t}_E is updated. Consequently, the two sets of equations are coupled and can advantageously be self-consistently solved using a double-loop procedure consisting of *macro*- and *micro*-iterations. In the *macro*-iterative step, we first solve the low-level amplitude equations to obtain the environment cluster amplitudes, T^E . We then construct the screened interaction for the fragment problem,

$$W^F = e^{-T^E} H e^{T^E}, \quad (13)$$

by similarity-transforming the bare Hamiltonian with T^E and subsequently restricting all indices to the fragment subspace. This operation typically generates effective Hamiltonian matrix elements with higher particle-rank

(many-body) contributions, i.e., although H is a two-body operator, W^F generally contains effective three-body and higher-body terms. In the *micro*-iterative step, we solve the fragment amplitude equations using W^F . The resulting fragment amplitudes, \mathbf{t}_F , enter the low-level amplitude equations and thereby update the next *macro*-iterative step. We also note that the W^F is typically denoted as a downfolded Hamiltonian, and Eq. (13) provides a static approach to build this quantity. A downfolded Hamiltonian can encapsulate the dynamical correlation effects of the environment into the fragment. As the number of degrees of freedom of the fragment problem is much smaller than the total system, we can treat the downfolded Hamiltonian with a higher-accuracy solver. A similar static approach was taken previously by Kowalski *et al.* to construct both unitary [40, 41] and non-unitary [35, 36] downfolded Hamiltonians, and Evangelista *et al.* [42] used a different framework, namely the driven similarity renormalization group (DSRG) approach, for this construction. However, unlike our work, these studies solved the downfolded Hamiltonian in isolation, that is, not self-consistently within an embedding framework.

In this work, we primarily focus on obtaining a higher accuracy solver for the fragment. Therefore, the necessary modifications to the solver will be elaborated in the following sections. We have also found that certain improvements to the low-level solver are necessary to achieve the desired accuracy from a high-level solver. Those improvements will also be discussed in the following sections.

B. Low-level methods for environment singles and doubles

The lower-order expansion in \tilde{H}^E allows us to choose various options for gaining a computational advantage, as was elaborated in our earlier work [37]. In the following, we will briefly explain the most useful approximation made, namely the relaxed scheme, which led to obtaining both qualitative and quantitative accuracy. Orbital relaxation of the environment was identified as vital, [28–30, 37], and according to the Thouless theorem [43], the e^{T_1} part of the CC ansatz can capture that effect. Therefore, a perturbation theory was defined in terms of the e^{T_1} transformed Hamiltonian, where the following partitioning was used:

$$\tilde{H} = e^{-T_1} H e^{T_1} = E_{\text{cl}} I + \tilde{F} + \tilde{V}, \quad (14)$$

where E_{cl} is the scalar (zero-body) contribution. Following an MP-type partitioning, we take \tilde{F} as the zeroth-order part and \tilde{V} as the first-order (fluctuation) contribution. We then define the first-order environment equa-

tions for the singles and doubles amplitudes as

$$\langle \Phi_\mu^E | \tilde{F} + [\tilde{F}, T_2] + [\tilde{F}, T_1] | \Phi_0 \rangle = 0, \mu = \binom{a}{i} \setminus \binom{A}{I}, \quad (15)$$

$$\langle \Phi_\mu^E | \tilde{V} + [\tilde{F}, T_2] | \Phi_0 \rangle = 0, \mu = \binom{ab}{ij} \setminus \binom{AB}{IJ}. \quad (16)$$

We refer to the embedding scheme that employs this set of environment equations as the MP1CC method.

In this work, we are also going to employ an improved variant of the environment treatment by including second-order terms in the perturbative equations, i.e.,

$$\langle \Phi_\mu^E | \tilde{F} + [\tilde{F}, T_1] + [\tilde{F} + \tilde{V}, T_2] | \Phi_0 \rangle = 0, \mu = \binom{a}{i} \setminus \binom{A}{I}, \quad (17)$$

$$\langle \Phi_\mu^E | \tilde{V} + [\tilde{F}, T_2] + [\tilde{V}, T_2] | \Phi_0 \rangle = 0, \mu = \binom{ab}{ij} \setminus \binom{AB}{IJ}. \quad (18)$$

We refer to the embedding scheme that employs this second-order set of environment equations as the MP2CC method. This approach increases the cost of the low-level step to $\mathcal{O}(N^6)$, compared to $\mathcal{O}(N^5)$ for MP1CC. As we shall see, this higher cost also yields improved accuracy in some strongly correlated problems.

C. CCSDT as a fragment solver

In this work, our goal is to solve the fragment problem using a method beyond CCSD. The fragment is described by the downfolded Hamiltonian mentioned in Eq. (13), where T^E consists of T_1^E , T_2^E amplitudes discussed above, defining:

$$W^F = e^{-T_1^E - T_2^E} H e^{T_1^E + T_2^E}. \quad (19)$$

The wavefunction ansatz for the fragment problem is further augmented with the triples amplitudes, such that it is CCSDT:

$$|\Psi^F\rangle = e^{T^F} |\Phi_0\rangle = e^{T_1^F + T_2^F + T_3^F} |\Phi_0\rangle, \quad (20)$$

where T_3^F denotes the fragment triples operator. This ansatz then substituted into Eq. (10) to derive the relevant projection equations. We note that the fragment Hamiltonian, Eq. (19), formally contains up to three-body terms. However, by suitable reordering of the tensor operations, they do not explicitly appear.

D. Complete neglect of environment triples

The environment triples amplitudes are treated perturbatively, in analogy with the truncated singles-doubles environment method. The definition of \tilde{H}^E is not straightforward when triple excitations are included, and we therefore investigate different approaches. In the simplest possible approach, we follow an argument from our previous work [37]: the MP1-level perturbation theory used to determine the environment amplitudes does not generate any T_3 contributions for a Hamiltonian that is at most two-body. We therefore set $T_3^E = 0$. In the CCSDT

method by Adamowicz *et. al* [44], a similar choice was made, and only active space triples were considered to be nonzero within CCSDT. We will therefore refer to this MPCC approach as MPCCSDT. The above method has an iterative $\mathcal{O}(V_F^5 O_F^3)$ cost for the fragment solver.

However, as noted previously in the context of CCSDT [45, 46] and corroborated by our numerical results here, some treatment of environment triples (T_3^E) is essential to obtain chemically accurate energetics. To that end, we have designed and implemented two perturbative schemes to describe the T_3^E amplitudes without fully evaluating their effect on the fragment Hamiltonian. One is single-shot non-iterative, denoted as MPCCSDT(pt), where the environment triples are fully decoupled from the fragment amplitude equations. The other allows leading order self-consistent coupling between the environment triples and fragment amplitudes based on an iterative perturbative procedure, which we denote as MPCCSDT(it). They are discussed in the following subsections.

E. Single-shot perturbation theory for environment triples

For the evaluation of environment triples amplitudes, we used a perturbative and noniterative formulation, as the lowest-order construction of these amplitudes requires an $\mathcal{O}(N^7)$ computational cost. In the interest of constructing a noniterative algorithm, we define W_F to be independent of T_3^E , so that the equations used to evaluate the fragment amplitudes are decoupled from the environment triple amplitudes. To derive the equation for T_3^E , we first apply the same similarity transformation of the Hamiltonian used for the singles-doubles amplitude equations, namely by e^{T_1} , and then partition the Hamiltonian in exactly the same manner as in Eq. (14).

Furthermore, unlike the SD equations, we exclude the \tilde{F}_{ov} term from the zeroth-order Hamiltonian and consider it as a first-order term, as we want to evaluate T_3^E in a non-iterative manner. Otherwise, the amplitude equation for T_2^E would contain an additional commutator term, $[\tilde{F}_{ov}, T_3^E]$, which would couple the T_3^E and T_2^E amplitude equations. Thus, the zeroth-order Hamiltonian consists of only \tilde{F}_{oo} and \tilde{F}_{vv} terms. The lowest-order environment triples amplitudes are then obtained from the following projection equation:

$$\langle \Phi_\mu^E | W_E + [\tilde{F}_{oo} + \tilde{F}_{vv}, T_3^{(1)}] | \Phi_0 \rangle = 0; \mu = \binom{abc}{ijk} \setminus \binom{ABC}{IJK}, \quad (21)$$

$$[\tilde{V}, T_2] + [\tilde{V}, T_3] = W_E \quad (22)$$

In this work, we further neglected the second commutator term containing the T_3 amplitudes, so that it does not generate a set of coupled equations, which is difficult to solve in a non-iterative manner. We also assume that its contribution is smaller than that of the commutator term containing the T_2 amplitudes. It should be noted that the terms in Eq. (22) are second-order perturbative terms. Thus, Eq. (21) is not fully consistent

with respect to the perturbation order when first-order amplitude equations are used for the SD ones. However, it is consistent when second-order amplitude equations are considered in that case. Nevertheless, we compare both combinations numerically, as they entail different computational costs for the SD equations.

Now, the contribution of T_3^E to the total energy can be derived as follows. We first notice that the contribution of T_3^E amplitudes to the residuals of T_1 and T_2 amplitudes was not taken into account, which for a full CCSDT computation would have vanished. This non-zero residual will contribute to the total energy, and it can be extracted from the CC Lagrangian:

$$\begin{aligned} \mathcal{L}_E &= \langle \Phi_0 | (1 + \Lambda_1 + \Lambda_2) [\tilde{V}, T_3^E] | \Phi_0 \rangle \\ &= \langle \Phi_0 | [(\Lambda_2 \tilde{V})_c, T_3^E] + [(\Lambda_1 \tilde{V})_{dc}, T_3^E] \\ &\quad + [(\Lambda_2 \tilde{F})_{dc}, T_3^E] | \Phi_0 \rangle \\ &= (\tilde{V}_{bc}^{ek} \lambda_{ae}^{ij} - \tilde{V}_{am}^{ij} \lambda_{bc}^{mk} + \tilde{V}_{ab}^{ij} \lambda_c^{jk} + \tilde{F}_a^i \lambda_{bc}^{jk})_E T_{ijk}^{abc,E} \\ &= Y_{abc,E}^{ijk} T_{ijk}^{abc,E} \end{aligned} \quad (23)$$

In the above equations, $(\dots)_c$ denotes the connected terms and $(\dots)_{dc}$ denotes the disconnected terms.

We further approximated $\Lambda_1 = T_1^\dagger$ and $\Lambda_2 = T_2^\dagger$ as leading-order contributions to the CC left eigenvectors. We will henceforth call this model MPCCSDT, that is, where all triples amplitudes are represented.

We can furthermore enhance our Lagrangian with this perturbative energy correction term and the amplitude equation Eq. (21) for the environment triples amplitudes, which constitutes the full Lagrangian for the MPCCSDT theory.

The energy expression derived in Eq. (23) has structural similarities with the ACCSD(T) method by Kucharski and Bartlett [47] and the triples approximated variant of the CCSD(2) method, namely CCSD(2)_T by Gwaltney and Head-Gordon [48]. However, those formulations differ from each other, and from the method discussed here in two ways: a) what form of the Hamiltonian, that is, similarity transformed or not, enters the equation, and b) what definition is used for T_3 . More specifically, in Eq. (21) we evaluate only environment amplitudes, where a fixed set of fragment T_3 amplitudes contributes a regularization term as will be shown in Eq. (25). Another distinction is that the T_1 and T_2 amplitudes that appear in Eq. (23) and (21) are optimized in the presence of T_3^F amplitudes. In their method of moment coupled cluster (MMCC) [49] formalism by Piecuch *et. al.* evaluate a similar energy correction due to the T_3 amplitudes, where an orbital non-invariant formula is derived based on the Epstein-Nesbet type denominator. Later, the same formalism was extended to evaluate energy correction on top of the CCSDt formalism, and the resulting method is called CC(t;3) [46]. Perhaps, CC(t;3) is the most closely related theory as our environment triples. Though some of the distinctions already mentioned above hold for the CC(t;3) method as

well. Moreover, in CC(t;3) formalism Hamiltonian moment was used for the $e^{T_1+T_2}$ transformed Hamiltonian. In comparison, we used only a e^{T_1} transformed Hamiltonian to evaluate the T_3 amplitudes in Eq. (21).

We will now elaborate on the solution strategy of Eq. (21): for a fixed set of T_3^F amplitudes, we aim to find the T_3^E amplitudes. Since \tilde{F} is generally a non-diagonal matrix, Eq. (21) presents a system of coupled equations of different T_3 amplitudes. Therefore, an iterative approach will be more suitable to solve this system of equations. However, this will incur an iterative $\mathcal{O}(N^7)$ cost of the above equations. In order to eliminate the iterative cost, we cast the equation in the following manner:

$$\begin{aligned} \langle \chi_{ijk,E}^{abc} | W_{ijk}^{abc} + [\tilde{F}, T_3^{LL}] + [\tilde{F}, T_3^{F,HL} - T_3^{F,LL}] | \Phi_0 \rangle \\ = \langle \chi_{ijk,E}^{abc} | \hat{W}_{ijk}^{abc} + [\tilde{F}, T_3^{LL}] | \Phi_0 \rangle \\ = 0 \end{aligned} \quad (24)$$

where, LL stands for the low-level method and HL stands for the high-level method or the previously obtained T_3^F amplitudes, $T_3 = T_3^F + T_3^E$ and $T_3^{F,LL}$ amplitudes are obtained from the following equations:

$$\langle \chi_{ijk}^{abc} | W_{ijk}^{abc} + [\tilde{F}, T_3^{LL}] | \Phi_0 \rangle = 0, \quad (25)$$

Now, Eq. (25) can be solved by transforming the \tilde{F} matrix into the semicanonical basis, and Eq. (24) can also be solved on the same semicanonical basis when we satisfy

$$\langle \chi_{ijk,F}^{abc} | W_{ijk}^{abc} + [\tilde{F}, T_3^{LL}] | \Phi_0 \rangle = 0 \quad (26)$$

in the original basis of that equation. This will modify Eq. (24) in the following way

$$\langle \chi_{ijk}^{abc} | \hat{W}_{ijk}^{abc} + [\tilde{F}, T_3^{LL}] | \Phi_0 \rangle = 0, \quad (27)$$

that is, we do not have any index restrictions now. As a result, Eq. (27) can be solved in a non-iterative manner by transforming it to a semicanonical basis, similar to Eq. (25). Thus, the evaluation of T_3^E can be summarized in four steps:

1. build W_{ijk}^{abc} from Eq. (22) using ERIs and converged T_1 , T_2 amplitudes,
2. solve Eq. (25) in a semicanonical basis to obtain $T_3^{F,LL}$ amplitudes,
3. construct \hat{W}_{ijk}^{abc} by using $T_3^{F,LL}$ and $T_3^{F,HL}$ amplitudes: $\hat{W}_{ijk}^{abc} = W_{ijk}^{abc} + ([\tilde{F}, T_3^{F,HL}] - [\tilde{F}, T_3^{F,LL}])$,
4. solve Eq. (27) in a semicanonical basis to obtain T_3^E amplitudes.

None of the above steps involves an iterative cost. An important aspect of this non-iterative method is that the semi-canonical basis obtained by diagonalizing the \tilde{F} matrix is biorthogonal, as \tilde{F} is not hermitian.

Since the above scheme takes all triples (fragment and environment) amplitudes into consideration and the T_3^E amplitudes are treated perturbatively, we will denote this method as MPCCSDT(pt).

F. Iterative perturbation theory for environment triples

In the perturbative treatment of environment triples amplitudes, we have neglected the influence of inactive triples on the fragment singles, doubles, and triples amplitudes. We consider that this particular kind of coupling may have significant contributions in the strongly correlated cases. To account for this coupling, we first solve the perturbative amplitude Eq. (21) for T_3^E amplitudes. The solution strategy remains the same as we have outlined in the previous section. We furthermore construct a modified fragment Hamiltonian by applying an additional similarity transformation of $e^{T_3^E}$ operator to the Hamiltonian. Therefore, the modified definition of the downfolded fragment Hamiltonian is:

$$W_F = e^{-T_1^E - T_2^E - T_3^E} H e^{T_1^E + T_2^E + T_3^E} \quad (28)$$

We apply this transformation in every *macro* iterative step to update the fragment Hamiltonian, W_F . Therefore, we will refer to this method as MPCCSDT(it). A closer analysis of Eq. (23) reveals that the energy contribution due to environment triples terms will be negligible now, which we will explain below. The amplitude equations for the T_1^F , T_2^F and T_3^F cluster operators in the MPCCSDt and MPCCSDT(pt) methods are formulated using the downfolded Hamiltonian defined in Eq. (19). Upon augmenting the additional terms to the downfolded Hamiltonian via Eq. (28), the fragment amplitude equations acquire extra residual contributions, that is, $\tilde{R} = R + R'$, where R' is the additional contribution to the previous residual R . By construction, \tilde{R} corresponds to the fragment subset of terms from the full CCSDT amplitude equation. In the self-consistent MPCCSDT(it) formulation, the fragment amplitudes are obtained by solving amplitude equations iteratively until $\tilde{R} \rightarrow 0$, as opposed to $R \rightarrow 0$ in the MPCCSDT(pt) and MPCCSDt methods. The term R' represents the fragment subset of terms of the $[\tilde{V}, T_3^E]$ commutator appearing in Eq. (23). This contribution vanishes for the MPCCSDT(it) method by virtue of the self-consistency condition mentioned above. However, in this method, we still neglect the total energy contribution from the environment subset of terms of the $[\tilde{V}, T_3^E]$ commutator. Thus, the influence of T_3^E amplitudes on the T_2^E and T_1^E amplitudes was not captured, which we assume to be negligible and is supported by numerical tests as well. We note that an analogous approximation is employed in the MPCCSD method.

The computational cost of evaluating the influence of T_3^E amplitudes on fragment amplitudes remains relatively low. Notably, the most expensive term in the CCSDT method, the particle-particle ladder (PPL) term, can now be evaluated with a cost of $V_F^3 O_F^3 V^2$, compared to the previous $V^5 O^3$. It also means that we need to evaluate only a subset of T_3^E amplitudes, for which the computational scaling will be $\mathcal{O}(V^3 V_F O_F^2 O)$. Additionally, the construction of these terms is required only during the

macro iterative step. Consequently, we have a prefactor of the number of macro iterations to the above computational scaling. However, the number of macro iterations is typically quite small, ranging from 5 to 10.

We have summarized the computational cost and the memory requirements of each of the methods in Table II.

III. IMPLEMENTATION

All the methodological developments described in the previous sections have been implemented in the PySCF [50–52] quantum chemistry package. The implementation of these variants is substantially more memory intensive and computationally more demanding than the MPCCSD method. We therefore employ three-center density-fitted (DF) electron repulsion integrals (ERIs) instead of the four-center ones when evaluating the triples amplitudes. In addition, we store only the fragment T_3 amplitudes in memory, while the environment T_3 amplitudes are handled using a disk-driven approach. The implementation of the MPCCSDT(it) scheme also requires the construction of fragment Hamiltonian matrix elements that involve tensor contractions between the bare Hamiltonian and the environment triples amplitudes (T_3^E). These terms are likewise implemented using a disk-driven approach. To implement Eq. (21), which is the low-level amplitude equation used to evaluate the T_3^E amplitudes, we introduce an approximation. As discussed in Sec. II E, a semicanonical basis is used to solve this equation perturbatively. However, this semicanonical basis is biorthogonal in nature because the Hamiltonian entering this equation is non-Hermitian. We do not perform an exact implementation using two different sets (left and right) of semicanonical orbitals for the transformation of the matrix elements, as has been done in the CCSD(2) work by Gwaltney *et. al.* [53]. Instead, we symmetrize the \tilde{F} matrix and construct the semicanonical basis from its diagonalization. This approach also avoids the appearance of complex semicanonical orbitals and complex eigenvalues and denominators. We have tested the validity of this approximation by comparing it with an iterative implementation of the same equation, which does not require the construction of a semicanonical basis. We observe a deviation of approximately 10^{-5} H, which is negligible. In future work, we aim to obtain a Hermitian Hamiltonian for the environment problem to avoid all the problems mentioned here.

IV. RESULTS

We will analyze various aspects of the newly proposed methods with two sets of applications: a) potential energy curves of the N_2 and F_2 molecules to examine the error versus full CCSDT at different bond distances; b) bond dissociation energies (BDE), and total atomization energies (TAE) of transition metal hydrides (TMH) and

Method	Macro	Micro	Perturbative	
UMP1CCSDt	Compute $\mathcal{O}(O^2V^2X)$	Memory $\max(\mathcal{O}(N^2X), \mathcal{O}(O^2V^2))$	Compute $\mathcal{O}(V_F^5O_F^3)$	Memory $\mathcal{O}(V_F^3O_F^3)$
UMP1CCSDT(pt)	$\mathcal{O}(V^2O^2X)$	$\mathcal{O}(V^3O)$	$\mathcal{O}(V_F^5O_F^3)$	$\mathcal{O}(V_F^3O_F^3)$
UMP1CCSDT(it)	$\mathcal{O}(V^3V_FO_F^2O)$	$\mathcal{O}(V^2OV_FO_F^2)$	$\mathcal{O}(V_F^5O_F^3)$	$\mathcal{O}(V_F^3O_F^3)$
UMP2CCSDt	$\mathcal{O}(O^2V^4)$	$\mathcal{O}(V^4)$	$\mathcal{O}(V_F^5O_F^3)$	$\mathcal{O}(V_F^3O_F^3)$
UMP2CCSDT(pt)	$\mathcal{O}(O^2V^4)$	$\mathcal{O}(V^4)$	$\mathcal{O}(V_F^5O_F^3)$	$\mathcal{O}(V_F^3O_F^3)$
UMP2CCSDT(it)	$\mathcal{O}(V^3V_FO_F^2O)$	$\mathcal{O}(V^2OV_FO_F^2)$	$\mathcal{O}(V_F^5O_F^3)$	$\mathcal{O}(V_F^3O_F^3)$

TABLE II. Compute and memory scaling for different methods at different steps of the methods. X denotes the size of the auxiliary basis set. We will denote the dimensionality of various sets of orbitals by the set itself, such as, $O_F \equiv |O_F|$, $V_F \equiv |V_F|$, etc.

a selected set of molecules from the W4-11 dataset [54], respectively.

A. Potential energy curves:

We will assess our triples embedding models for N_2 and F_2 potential energy curves by measuring deviations against unrestricted CCSDT (UCCSDT). For both N_2 and F_2 , the UCCSD error is quite large, which allows us to meaningfully investigate the role of triples. The cc-pCVTZ basis is chosen to be the large target basis, so our reference calculations are UCCSDT/cc-pCVTZ. Following our previous work, we have chosen the AVAS scheme to construct the fragment basis. Within this scheme, we chose cc-pVDZ to define the space of active orbitals, which previously yielded good performance in the MPCCSD method.

Fig. 1 plots the error in N_2 interaction energies ($E_{mol} - 2 * E_{atom}$) for each method versus bond length for this triple bond stretching problem, using UHF orbitals to ensure correct dissociation. In the equilibrium region, the CCSD(T) method performs very well, with < 1 mH error. As we further stretch the bond, entering the spin-recoupling region, CCSD(T) exhibits poor behavior, and attains a non-parallelity error (NPE) of 13 mH. We also observe a first derivative discontinuity in the CCSD(T) error curve near the equilibrium region, at the Coulson-Fischer point, as expected for a perturbative method [55].

Moving on to the embedding schemes, we observe that the UCCSD(T) error in the spin-recoupling region is significantly reduced for all the variants. With the MPCCSDt methods (solid curves), where we employ CCSDT only for the fragment, NPE is reduced by ~ 2 mH (UMP1CCSDt) and ~ 3.5 mH (UMP2CCSDt), which is encouraging. However, the remaining NPE is still chemically relevant, and is attributable to neglect of environment triples amplitudes. This is proven by including the environmental triples contribution perturbatively via the UMPCCSDT(pt) method (dot-dashed curves), which greatly reduces the error at every bond distance. Even then, the performance of our environmental triples scheme is not completely satisfactory, as a change in sign occurs in the error curve and a ~ 3.5 mH NPE remains in the interaction energy curve. When we introduce the cou-

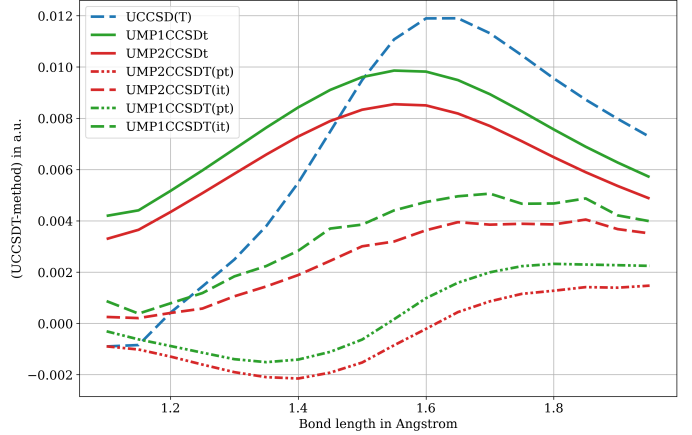


FIG. 1. Electronic energy error with respect to UCCSDT along a PEC for N_2 in the cc-pCVTZ basis set. AVAS active space is constructed with cc-pVDZ basis set. We set the energy at dissociation as the zero energy for each method.

pling between the fragment and the environment triples (T_3^E) amplitudes via the UMPCCSDT(it) methods, the error curve looks better behaved, as there is no change in sign. Note that the UMPCCSDT(it) curves are not completely smooth, which we have found is due to using density fitted integrals in the evaluation of T_3^E amplitudes (Fig. S1). Note that the choice of the low-level method does not significantly affect the error curve, in comparison to other factors.

Next, we examine the single-bond stretching of the F_2 molecule using the potential energy curves shown in Fig. 2. Many of the trends observed in the N_2 study persist in this case. Specifically, (a) the CCSD(T) method performs reasonably well at short bond lengths but becomes increasingly unreliable as the bond is stretched; and (b) employing CCSDT as the fragment solver substantially reduces the NPE to 9 mH. This indicates that the missing dynamical correlation arising from environmental triples is even more critical for F_2 than for N_2 . Indeed, upon including the environmental triples correction, the NPE is further reduced to 4 mH. Nevertheless, we find that incorporating the T_3^E amplitudes perturbatively is insufficient to fully eliminate the pronounced deviations observed in the bond-length range of 1.6–2.0 Å. We did not

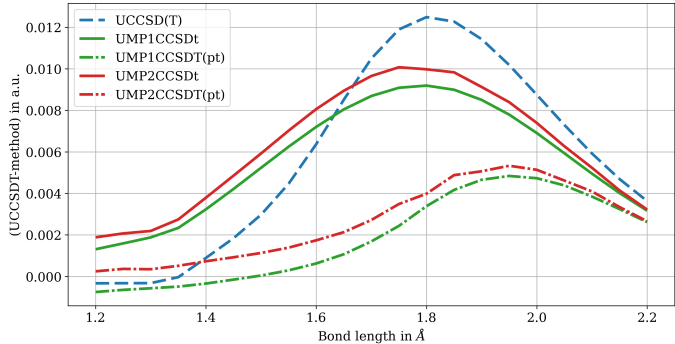


FIG. 2. Electronic energy error with respect to UCCSDT along a PEC for F_2 in the cc-pCVTZ basis set. AVAS active space is constructed with cc-pVDZ basis set. We set the energy at dissociation as the zero energy for each method.

perform UMPCCSDT(it) calculations for F_2 in light of the non-smoothness issue encountered above for N_2 .

B. Total atomization energy comparison:

We will now discuss the performance of our method by evaluating the total bond dissociation energy (BDE) of a few 3d transition metal hydrides and the total atomization energy (TAE) of three triatomic molecules from the W4-11 dataset.

1. Transition metal hydrides:

We selected MnH, CrH, CoH and FeH molecules, which are challenging due to the presence of both static and dynamical correlation effects [56, 57], scalar relativistic effects [58, 59] and significant basis set effects [60]. We focus on the electron correlation problem, and thus use the non-relativistic Hamiltonian, with a large enough basis set (cc-pwCVTZ for the transition metals (TMs) and cc-pVDZ for the H atom). We do not freeze any orbitals, as core-valence correlation is significant [59], and we want to investigate a low-level treatment of the core orbitals via embedding. The active (fragment) space excludes the Ne core of the TM atoms. The def2-SV(P) basis set was chosen within the AVAS scheme to generate fragment orbitals, which includes 5s, 4p, 4d orbitals in addition to the valence atomic orbitals, in order to capture key dynamical correlations with the fragment solver. For the MnH, FeH and CoH molecules, the equilibrium geometry is taken from [57], and the structure of CrH is taken from [58]. We again employ unrestricted orbitals and cluster amplitudes for all the molecules unless otherwise stated.

The results are summarized in Tables III (singles and doubles only) and IV (with triples). MnH is in the high-spin septet state (${}^7\Sigma^+$), and Mn is also high-spin (6S). These high-spin configurations should make the electronic structure relatively straightforward: the

total triples contribution to the BDE is small (~ 4 kJ/mol), and CCSD(T) recovers it almost completely. We next consider the embedding schemes, where it turns out that things are not so straightforward. The first-order (MP1) low-level method within the MP1CCSDt scheme reproduces the BDE very well. However, when we improve the embedding by including environment triples, either perturbatively (UMP1CCSDT(pt)) or iteratively (UMP1CCSDT(it)), the agreement deteriorates! It also deteriorates when the (better) second-order (MP2) low-level method is used within the MP2CCSDt scheme. This indicates a fortuitous error cancellation in UMP1CCSDt, which is supported by comparing total energies against CCSDT (Table SI). Both UMP1CCSDT(pt) and UMP1CCSDT(it) substantially overestimate the correlation energy (by more than 10 mH) for both MnH and Mn. By contrast, with MP2 environment singles and doubles, the inclusion of environment triples, via UMP2CCSDT(pt) or (it), reduces the BDE error to less than 0.5 kJ/mol, or about a seven-fold reduction from 3.4 kJ/mol error in UMP2CCSDt. We conclude that second-order treatment of environment singles and doubles is necessary for even the seemingly easy case of MnH.

TABLE III. Bond Dissociation Energies (BDE) of the transition metal hydrides at the CCSD level in kJ/mol. We have compared two variants of the low-level theory, denoted as MP1 and MP2. BDE is reported at the CCSD level, and for the approximate methods, the differences w.r.t. CCSD were provided.

Method	MnH	CrH	CoH	FeH
CCSD	152.90	192.32	236.23	252.80
UMP1CCSD	3.75	-0.10	16.66	14.04
UMP2CCSD	-0.21	-0.07	-1.47	-2.24

TABLE IV. Bond Dissociation Energies (BDE) of the transition metal hydrides at the CCSDT level in kJ/mol. Two variants of the low-level method (MP1 and MP2) and a few variants of the embedded triples method reported in Sec. II C were compared. BDE is reported at the CCSDT level, and for the approximate methods, the errors w.r.t. CCSDT were provided. The large basis set used is cc-pwCVTZ, and the small basis set used to construct the active space is def2-sv(p). We have applied a Ne core when the fragment space is constructed.

Method	MnH	CrH	CoH	FeH
CCSDT	148.81	201.72	247.34	256.03
CCSD(T)	0.54	7.42	35.83	14.91
UMP1CCSDt	0.71	6.21	22.42	13.73
UMP1CCSDT(pt)	4.77	0.72	33.06	23.92
UMP1CCSDT(it)	3.49	1.36	14.98	18.71
UMP2CCSDt	-3.40	4.23	4.69	-2.31
UMP2CCSDT(pt)	0.32	-0.93	6.04	1.63
UMP2CCSDT(it)	-0.47	0.58	2.24	0.85

Next, we consider the ${}^6\Sigma^+$ state of the CrH molecule, which comprises five unpaired parallel spins and one pair

of coupled spins in the valence shell. As a result, CrH exhibits a more complex electronic structure than MnH. This complexity is reflected in the total BDE, which at the CCSD level is approximately 9 kJ/mol lower than that obtained with the CCSDT method. The CCSD(T) method recovers only about 2 kJ/mol of the triples correction, which is not satisfactory. When we apply the embedding method with an MP1-level treatment of the environment SD amplitudes, the total BDE is reproduced more accurately at the UMP1CCSDt level than with CCSD(T). By including the environment triples contribution, either perturbatively or iteratively, we achieve nearly the same accuracy as CCSDT (~ 1 kJ/mol error). Unsurprisingly, using the improved UMP2CCSDT methods leads to only marginal improvements in the BDE. Overall, CrH represents a relatively straightforward case for the embedding methods, and all variants show satisfactory performance.

FeH has a $^4\Delta$ ground state, with three unpaired parallel spins and three pairs of coupled spins in the valence shell. Although the triples contribution to the BDE is relatively small, ~ 3.2 kJ/mol, FeH exhibits interesting behavior when approximate methods are applied. For example, the deviation of CCSD(T) from CCSDT is significantly larger (15 kJ/mol) than that of CCSD. This is because the perturbative triples correction cannot restore the broken spin symmetry introduced by the UHF reference. In contrast, when the BDE is evaluated using a restricted open-shell Hartree-Fock (ROHF) reference, the difference between CCSDT and CCSD(T) is reduced more than three-fold to ~ 4 kJ/mol. Turning to the embedding approaches, employing MP1 as the low-level treatment for the SD amplitudes leads to a significant deviation at the UMP1CCSD level. This deviation is recovered only when the improved perturbative method, UMP2CCSD, is used as the low-level treatment. A similar trend is observed when comparing the triples variants of the embedding methods. Notably, the second-order variant of the low-level SD treatment performs consistently well across all triples variants, in a way that is similar to what we saw with MnH.

CoH ($^3\Phi$ ground state) is the most challenging of our 4 TM hydrides. The 11 kJ/mol triples contribution is three times smaller than the CCSD(T) error (36 kJ/mol) with UHF orbitals. This is a more drastic version of the failure of CCSD(T) discussed above for FeH, and again can be remedied with an ROHF reference, which reduces the CCSD(T) error to ~ 0.5 kJ/mol. Like FeH, we find that the second-order variants (UMP2CCSDt and UMP2CCSDT) perform much better than their first-order cousins. Unlike FeH, however, the iterative evaluation of T_3^E is significantly (~ 4 kJ/mol) more accurate than the corresponding perturbative treatment.

2. Strongly correlated systems from the W4-11 dataset:

We analyzed the total atomization energy (TAE) of three triatomic molecules from the W4-11 dataset, FO_2 , O_3 , and NO_2 . For these molecules, the improvement obtained with CCSD(T) is so exceptionally large (~ 15 kcal/mol) that they are often regarded as multireference systems even in their ground states. We employed the cc-pCVTZ basis set as the large basis for all atoms and the cc-pVDZ basis set as the minimal basis to construct the active space using the AVAS scheme. In our earlier work [37], we showed that an MP1-level treatment of the environment SD amplitudes is sufficient to recover TAE within chemical accuracy for the UMPCCSD method.

In this work, we compared a few variants of the embedding method combined with the triples solver (Table V), where the low-level method corresponds to the two variants discussed in Sec. II B. For all three molecules, both low-level methods perform equally well with the SDT solver, consistent with the behavior observed for the SD solver. Apparently, the complexities of the TM hydrides are not an issue here. Even when we neglect the environment triples contribution within the embedding approach, we obtain an accuracy comparable to that of the CCSD(T) method, except for the NO_2 molecule. In that case, CCSD(T) performs so well as to be nearly unbeatable, while the UMP2CCSDT embedding methods reduces the CCSD(T) error by more than a factor of ten for FO_2 and O_3 . We note that our (UCCSDT-UCCSD(T)) difference is much larger than that previously reported [61], probably because we retain the full core and not resort to composite approaches to obtain the UCCSDT energies.

TABLE V. Total Atomization Energies (TAE) in kcal/mol for FO_2 , O_3 and NO_2 molecules. Two variants of the low-level method (MP1 and MP2) and a few variants of the embedded triples method reported in Sec. II C were compared. TAE is reported at the CCSDT level, and for the approximate methods and CCSD, the errors w.r.t. CCSDT were provided. The large basis set used is cc-pCVTZ, and the small basis set used to construct the active space is cc-pVDZ.

Method	FO_2	O_3	NO_2
UCCSDT	121.83	132.36	212.83
UCCSD	18.93	21.35	17.56
UCCSD(T)	4.40	5.41	-0.51
UMP1CCSDt	5.35	5.73	3.33
UMP1CCSDT(pt)	-0.51	-0.62	-2.60
UMP2CCSDt	5.92	7.17	3.47
UMP2CCSDT(pt)	0.23	0.43	-1.58

V. CONCLUSION

We have developed, implemented, and numerically explored several variants of a triples extension of our static embedding scheme, MPCC [37]. These MPCC embed-

ding methods use a coupled cluster singles, doubles, and triples (CCSDT) solver in an active (fragment) region, coupled to a lower order Møller-Plesset (MP) perturbative treatment of the environment. This higher-accuracy CCSDT solver enabled us to achieve both qualitative and quantitative accuracy beyond the CCSD and CCSD(T) level on various problems. Examples of such applications include radical chemistry and transition metal chemistry.

However, the inclusion of a CCSDT solver introduces the challenge that the feedback from the environment must be adequately captured when triples are introduced in the fragment. Within the MPCCSD scheme, we captured the feedback of the (first order) environment SD amplitudes on the fragment SD amplitudes to all orders of perturbation, while the feedback of the fragment amplitudes on the environment amplitudes was included at first order. Unfortunately, treating environment triples on the same footing as environment doubles is not feasible due to the steep scaling of triples in both memory and computational cost.

Instead, as summarized in Table II, we explored three approximate schemes to handle the environment triples, and their influence on the active fragment. These schemes involve macroiterations to update the environment amplitudes, microiterations to update the fragment amplitudes, and (sometimes) a final non-iterative step.

1. The simplest possible approach is to completely neglect the environment triples, leading to MPCCSDt, where the lowercase “t” indicates that only fragment triples are included.
2. The next simplest approach is MPCCSDT(pt), wherein we neglect the influence of environment triples on the fragment amplitudes. The environment triples are described by a second-order amplitude equation, in which the fragment singles, doubles and triples amplitudes all contribute to the environment triples (neglecting the $[V, T_3]$ terms to avoid their $\mathcal{O}(V^5 O^3)$ computational cost). The resulting equations are solved by semicanonicalizing the orbital basis.
3. In the most advanced approach, MPCCSDT(it), we also account for the influence of environment triples on the fragment amplitudes, which modifies the fragment Hamiltonian through an additional similarity transformation by the environment triples. This procedure incurs a macro iterative $\mathcal{O}(N^7)$ cost.

Each of these 3 methods can evaluate the SD amplitudes using first-order low-level equations (MP1) as used in our earlier work, or, at additional compute cost, by also including second-order terms in the resulting MP2 equations. The MP2 equations are consistent in terms of the perturbative order with the low-level treatment used for the environment triples amplitudes. Thus, we have a total of 6 candidate embedded triples methods (Table II).

The 6 different candidate MPCCSDT methods were then numerically tested on: a) bond-stretching of N_2 and F_2 ; b) TAEs of three multi-reference systems: FO_2 , O_3 , and NO_2 ; c) BDE analysis of 4 transition metal hydrides: MnH , CrH , FeH and CoH . The fragment was defined by a medium-sized basis set (cc-pVDZ) with a neon core excluded for the transition metals, while the environment contained any frozen orbitals and additional orbitals from a larger basis set (cc-pwCVTZ for TMs, and otherwise cc-pCVTZ). Unrestricted orbitals were used throughout. The major findings were:

1. The neglect of environment triples via either MP1CCSDt or MP2CCSDt typically leads to unacceptably large errors, and therefore cannot be recommended.
2. Generally, we recommend the MP2CCSDT(pt) approach over MP1CCSDT(pt). MP2CCSDT(pt) almost always significantly outperforms CCSD(T), often reducing CCSD(T) errors in strongly correlated cases by over a factor of 10, while having the same rate-determining compute cost in the limit of a large environment.
3. In the most strongly correlated molecules, such as CoH , FeH , the use of second order environment amplitudes is important, and MP2CCSDT(pt) significantly outperforms MP1CCSDT(pt). In other cases the difference is smaller. CoH and FeH are also the only cases we examined where MP2CCSDT(it) significantly improves upon MP2CCSDT(pt), with up to 2.5 times error reduction.

Although we have identified a systematic way to improve the accuracy of the UMPCCSDT method, several aspects require further development. Improved scaling could be achieved by adopting linear scaling methods for the perturbative environment amplitudes[62], or conceivably also the fragment solver. Many strong correlation problems, such as the ones involving multiple metal centres, for example, cubane, Fe-Mo cofactor of the nitrogenase enzyme, may need a solver that incorporates higher-order correlations than CCSDT. To this end, we aim to incorporate a selected configuration interaction (sCI) [23, 63–66] method and quantum hardware-inspired quantum subspace diagonalization (QSD) [67, 68] method as a solver in the future.

VI. ACKNOWLEDGEMENTS

This material is based upon work supported by the U.S. Department of Energy, Office of Science, Office of Advanced Scientific Computing Research and Office of Basic Energy Sciences, Scientific Discovery through Advanced Computing (SciDAC) program under Award Number DE-SC0022198 (A.S., K.B.W. and L.L.), and Award Number DE-SC0022364 (M.H-G.). This research

used resources of the National Energy Research Scientific Computing Center, a DOE Office of Science User

Facility supported by the Office of Science of the U.S. Department of Energy under Contract No. DE-AC02-05CH11231 using NERSC award BES-ERCAP0029462.

[1] P.-O. Löwdin, *Advances in Physics* **5**, 1 (1956).

[2] W. J. Hehre, R. Ditchfield, L. Radom, and J. A. Pople, *Journal of the American Chemical Society* **92**, 4796 (1970).

[3] M. J. Frisch, R. Krishnan, and J. A. Pople, *Chemical Physics Letters* **75**, 66 (1980).

[4] J. Čížek, *J. Chem. Phys.* **45**, 4256 (1966), <http://dx.doi.org/10.1063/1.1727484>.

[5] J. Paldus, J. Čížek, and I. Shavitt, *Phys. Rev. A* **5**, 50 (1972).

[6] K. Raghavachari, G. W. Trucks, J. A. Pople, and M. Head-Gordon, *Chem. Phys. Lett.* **157**, 479 (1989).

[7] S. M. Casey and D. G. Leopold, *The Journal of Physical Chemistry* **97**, 816 (1993).

[8] Z. Fang, M. Vasiliu, K. A. Peterson, and D. A. Dixon, *Journal of Chemical Theory and Computation* **13**, 1057 (2017).

[9] L. W. Bertels, J. Lee, and M. Head-Gordon, *Journal of Chemical Theory and Computation* **17**, 742 (2021).

[10] Z. Fang, Z. Lee, K. A. Peterson, and D. A. Dixon, *Journal of Chemical Theory and Computation* **12**, 3583 (2016).

[11] Y. S. Al-Hamdani, P. R. Nagy, A. Zen, D. Barton, M. Kállay, J. G. Brandenburg, and A. Tkatchenko, *Nature Communications* **12**, 3927 (2021).

[12] N. Masios, A. Irmler, T. Schäfer, and A. Grüneis, *Phys. Rev. Lett.* **131**, 186401 (2023).

[13] T. Schäfer, A. Irmler, A. Gallo, and A. Grüneis, *Nature Communications* **16**, 9108 (2025).

[14] S. A. Kucharski and R. J. Bartlett, *The Journal of Chemical Physics* **108**, 9221 (1998).

[15] R. P. Steele, R. A. DiStasio, Y. Shao, J. Kong, and M. Head-Gordon, *The Journal of chemical physics* **125** (2006).

[16] R. P. Steele and M. Head-Gordon, *Molecular Physics* **105**, 2455 (2007).

[17] R. P. Steele, R. A. DiStasio Jr, and M. Head-Gordon, *Journal of Chemical Theory and Computation* **5**, 1560 (2009).

[18] Liang and M. Head-Gordon, *The Journal of Physical Chemistry A* **108**, 3206 (2004).

[19] A. Georges and G. Kotliar, *Phys. Rev. B* **45**, 6479 (1992).

[20] A. Georges, G. Kotliar, W. Krauth, and M. J. Rozenberg, *Rev. Mod. Phys.* **68**, 13 (1996).

[21] G. Knizia and G. K.-L. Chan, *Phys. Rev. Lett.* **109**, 186404 (2012).

[22] G. Knizia and G. K.-L. Chan, *J. Chem. Theory Comput.* **9**, 1428 (2013), pMID: 26587604.

[23] N. M. Tubman, C. D. Freeman, D. S. Levine, D. Hait, M. Head-Gordon, and K. B. Whaley, *Journal of Chemical Theory and Computation* **16**, 2139 (2020).

[24] T. Zhu, C. A. Jiménez-Hoyos, J. McClain, T. C. Berkelbach, and G. K.-L. Chan, *Phys. Rev. B* **100**, 115154 (2019).

[25] T. Zhu and G. K.-L. Chan, *Phys. Rev. X* **11**, 021006 (2021).

[26] A. Shee and D. Zgid, *J. Chem. Theory Comput.* **15**, 6010 (2019).

[27] M. Welborn, T. Tsuchimochi, and T. V. Voorhis, *J. Chem. Phys.* **145**, 074102 (2016), <http://dx.doi.org/10.1063/1.4960986>.

[28] M. Nooijen, *The Journal of Chemical Physics* **111**, 10815 (1999).

[29] A. D. Bochevarov and C. D. Sherrill, *The Journal of chemical physics* **122** (2005).

[30] A. D. Bochevarov, B. Temelso, and C. D. Sherrill, *The Journal of chemical physics* **125** (2006).

[31] P. Piecuch, N. Oiphant, and L. Adamowicz, *The Journal of chemical physics* **99**, 1875 (1993).

[32] P. Piecuch and L. Adamowicz, *The Journal of chemical physics* **100**, 5792 (1994).

[33] R. H. Myhre, A. M. J. Sánchez de Merás, and H. Koch, *J. Chem. Phys.* **141**, 224105 (2014).

[34] S. D. Folkestad, E. F. Kjønstad, L. Goletto, and H. Koch, *J. Chem. Theory Comput.* **17**, 714 (2021).

[35] K. Kowalski, *The Journal of Chemical Physics* **148**, 094104 (2018).

[36] K. Kowalski, *J. Chem. Phys.* **158**, 054101 (2023).

[37] A. Shee, F. M. Faulstich, K. B. Whaley, L. Lin, and M. Head-Gordon, *The Journal of Chemical Physics* **161**, 164107 (2024).

[38] J. Noga and R. J. Bartlett, *The Journal of Chemical Physics* **86**, 7041 (1987).

[39] E. R. Sayfutyarova, Q. Sun, G. K.-L. Chan, and G. Knizia, *J. Chem. Theory Comput.* **13**, 4063 (2017).

[40] N. P. Bauman, E. J. Bylaska, S. Krishnamoorthy, G. H. Low, N. Wiebe, C. E. Granade, M. Roetteler, M. Troyer, and K. Kowalski, *J. Chem. Phys.* **151**, 014107 (2019).

[41] M. Metcalf, N. P. Bauman, K. Kowalski, and W. A. de Jong, *Journal of Chemical Theory and Computation* **16**, 6165 (2020).

[42] R. Huang, C. Li, and F. A. Evangelista, *PRX Quantum* **4**, 020313 (2023).

[43] D. J. Thouless, *Nuclear Physics* **21**, 225 (1960).

[44] L. Adamowicz, P. Piecuch, and K. B. Ghose, *Molecular Physics* **94**, 225 (1998).

[45] J. Shen, E. Xu, Z. Kou, and S. Li, *The Journal of Chemical Physics* **132**, 114115 (2010).

[46] J. Shen and P. Piecuch, *J. Chem. Theory Comput.* **8**, 4968 (2012), <https://doi.org/10.1021/ct300762m>.

[47] A. G. Taube and R. J. Bartlett, *The Journal of Chemical Physics* **128**, 044110 (2008).

[48] S. R. Gwaltney and M. Head-Gordon, *The Journal of Chemical Physics* **115**, 2014 (2001).

[49] P. Piecuch, K. Kowalski, I. S. O. Pimienta, and M. J. McGuire, *International Reviews in Physical Chemistry* **21**, 527 (2002).

[50] Q. Sun, *Journal of computational chemistry* **36**, 1664 (2015).

[51] Q. Sun, T. C. Berkelbach, N. S. Blunt, G. H. Booth, S. Guo, Z. Li, J. Liu, J. D. McClain, E. R. Sayfutyarova, S. Sharma, *et al.*, *Wiley Interdisciplinary Reviews: Com-*

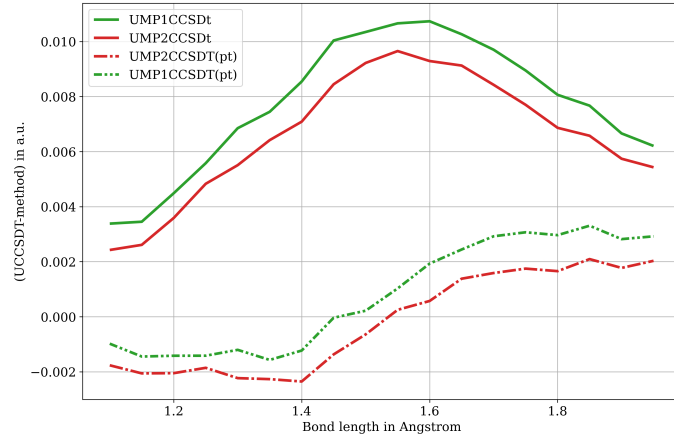


FIG. S1. Interaction energy error with respect to UCCSDT along a PEC for N_2 in the cc-pCVTZ basis set. AVAS active space is constructed with the cc-pVDZ basis set. Density-fitted integrals are used for all the methods described here.

putational Molecular Science **8**, e1340 (2018).

[52] Q. Sun, X. Zhang, S. Banerjee, P. Bao, M. Barbry, N. S. Blunt, N. A. Bogdanov, G. H. Booth, J. Chen, Z.-H. Cui, *et al.*, The Journal of chemical physics **153** (2020).

[53] S. R. Gwaltney, C. D. Sherrill, M. Head-Gordon, and A. I. Krylov, *Journal of Chemical Physics* **113**, 3548 – 3560 (2000).

[54] A. Karton, S. Daon, and J. M. Martin, *Chem. Phys. Lett.* **510**, 165 (2011).

[55] W. Kurlancheck and M. Head-Gordon, *Mol. Phys.* **107**, 1223 (2009).

[56] D. Hait, N. M. Tubman, D. S. Levine, K. B. Whaley, and M. Head-Gordon, *Journal of chemical theory and computation* **15**, 5370 (2019).

[57] A. Waigum, M. Ertürk, and A. Köhn, *The Journal of Physical Chemistry A* **128**, 10053 (2024), pMID: 39535968.

[58] X. Xu, W. Zhang, M. Tang, and D. G. Truhlar, *Journal of Chemical Theory and Computation* **11**, 2036 (2015), pMID: 26574408.

[59] L. Cheng, J. Gauss, B. Ruscic, P. B. Armentrout, and J. F. Stanton, *Journal of Chemical Theory and Computation* **13**, 1044 (2017), pMID: 28080054.

[60] Z. Fang, M. Vasiliu, K. A. Peterson, and D. A. Dixon, *Journal of Chemical Theory and Computation* **13**, 1057 (2017), pMID: 28080051.

[61] E. Semidalas, A. Karton, and J. M. L. Martin, *The Journal of Physical Chemistry A* **128**, 1715 (2024).

[62] Z. Wang, H. Ling, T. Shi, Y. Shen, Z. Wang, Y. Liu, X. S. Li, and M. Head-Gordon, *Journal of Chemical Theory and Computation* **21**, 10910 (2025).

[63] F. A. Evangelista, *The Journal of Chemical Physics* **140**, 124114 (2014).

[64] A. A. Holmes, N. M. Tubman, and C. J. Umrigar, *Journal of Chemical Theory and Computation* **12**, 3674 (2016).

[65] Y. Garniron, A. Scemama, P.-F. Loos, and M. Caffarel, *The Journal of Chemical Physics* **147**, 034101 (2017).

[66] S. J. Cotton, *The Journal of Chemical Physics* **157** (2022).

[67] Y. O. Nakagawa, M. Kamoshita, W. Mizukami, S. Sudo, and Y.-y. Ohnishi, *Journal of Chemical Theory and Computation* **20**, 10817 (2024).

[68] J. Robledo-Moreno, M. Motta, H. Haas, A. Javad-Abhari, P. Jurcevic, W. Kirby, S. Martiel, K. Sharma, S. Sharma, T. Shirakawa, I. Sitedikov, R.-Y. Sun, K. J. Sung, M. Takita, M. C. Tran, S. Yunoki, and A. Mezzacapo, *Science Advances* **11**, eadu9991 (2025).

Supplemental Information

I. THE EFFECT OF DENSITY FITTED INTEGRALS IN THE POTENTIAL ENERGY CURVE OF N_2

We have analyzed the effect of using density-fitted integrals in the study of the potential energy curve of the N_2 molecule in Fig. S1. We observe that when DF integrals are used for iterative UMP1CCSDt and UMP2CCSDt methods, the error curve w.r.t. the CCSDT method is not smooth. As a result, when the environment triples correction is added to those methods via the UMP1CCSDT(pt) and UMP2CCSDT(pt) methods, the same error curve again appeared to be non-smooth. Therefore, we decided to plot those curves using the non-DF integrals. Furthermore, we observe the same non-smoothness when tried to capture the environment triples corrections iteratively. However, in that case, we avoided performing the same calculation.

II. FURTHER ANALYSIS OF THE TRANSITION METAL HYDRIDE MOLECULES

In order to facilitate further analysis of the TMH results presented in Table IV, we have provided two additional tables in this section - one that reports the BDE values at the CCSD, CCSD(T) and CCSDT level, starting from the ROHF MO basis, and the other showing the total energy values at various levels of theory.

TABLE SI. Total energies (in Hartree) for MnH, Mn, and H obtained with different coupled-cluster methods.

Method	MnH	Mn	H
UCCSDT	-1151.191 79	-1150.635 83	-0.499 28
UCCSD	-1151.176 91	-1150.619 39	-0.499 28
UCCSD(T)	-1151.191 78	-1150.636 03	-0.499 28
UMP1CCSD	-1151.186 90	-1150.630 82	-0.499 28
UMP2CCSD	-1151.170 85	-1150.613 26	-0.499 28
UMP1CCSDt	-1151.188 91	-1150.633 22	-0.499 28
UMP1CCSDT(pt)	-1151.203 15	-1150.649 08	-0.499 28
UMP1CCSDT(it)	-1151.193 94	-1150.639 32	-0.499 28
UMP2CCSDt	-1151.172 81	-1150.615 56	-0.499 28
UMP2CCSDT(pt)	-1151.185 95	-1150.630 11	-0.499 28
UMP2CCSDT(it)	-1151.177 11	-1150.620 97	-0.499 28

TABLE SII. Total energies (in Hartree) for CrH, Cr, and H obtained with different coupled-cluster methods.

Method	CrH	Cr	H
UCCSDT	-1044.652 13	-1044.076 03	-0.499 28
UCCSD	-1044.633 32	-1044.060 79	-0.499 28
UCCSD(T)	-1044.649 68	-1044.076 40	-0.499 28
UMP1CCSD	-1044.644 20	-1044.071 63	-0.499 28
UMP2CCSD	-1044.626 73	-1044.054 17	-0.499 28
UMP1CCSDt	-1044.647 45	-1044.073 71	-0.499 28
UMP1CCSDT(pt)	-1044.664 71	-1044.088 88	-0.499 28
UMP1CCSDT(it)	-1044.654 25	-1044.078 66	-0.499 28
UMP2CCSDt	-1044.630 78	-1044.056 28	-0.499 28
UMP2CCSDT(pt)	-1044.646 37	-1044.069 90	-0.499 28
UMP2CCSDT(it)	-1044.636 50	-1044.060 61	-0.499 28

TABLE SIII. Total energies (in Hartree) for FeH, Fe, and H obtained with different coupled-cluster methods.

Method	FeH	Fe	H
UCCSDT	-1263.869 04	-1263.272 24	-0.499 28
UCCSD	-1263.846 51	-1263.250 94	-0.499 28
UCCSD(T)	-1263.863 92	-1263.272 81	-0.499 28
UMP1CCSD	-1263.864 59	-1263.274 38	-0.499 28
UMP2CCSD	-1263.838 64	-1263.242 23	-0.499 28
UMP1CCSDt	-1263.869 26	-1263.277 69	-0.499 28
UMP1CCSDT(pt)	-1263.887 07	-1263.299 39	-0.499 28
UMP1CCSDT(it)	-1263.875 20	-1263.285 53	-0.499 28
UMP2CCSDt	-1263.843 57	-1263.245 89	-0.499 28
UMP2CCSDT(pt)	-1263.860 62	-1263.264 44	-0.499 28
UMP2CCSDT(it)	-1263.849 35	-1263.252 88	-0.499 28

TABLE SIV. Total energies (in Hartree) for CoH, Co, and H obtained with different coupled-cluster methods.

Method	CoH	Co	H
UCCSD	-1382.904 18	-1382.314 92	-0.499 28
UCCSD(T)	-1382.919 24	-1382.339 40	-0.499 28
UCCSDT	-1382.931 88	-1382.338 40	-0.499 28
UMP1CCSD	-1382.931 65	-1382.348 74	-0.499 28
UMP2CCSD	-1382.894 62	-1382.304 80	-0.499 28
UMP1CCSDt	-1382.937 64	-1382.352 69	-0.499 28
UMP1CCSDT(pt)	-1382.958 06	-1382.377 16	-0.499 28
UMP1CCSDT(it)	-1382.944 14	-1382.356 36	-0.499 28
UMP2CCSDt	-1382.901 03	-1382.309 33	-0.499 28
UMP2CCSDT(pt)	-1382.920 85	-1382.329 66	-0.499 28
UMP2CCSDT(it)	-1382.909 85	-1382.317 22	-0.499 28

TABLE SV. Bond dissociation energies (in kJ/mol) for MnH, CrH, CoH and FeH obtained with RO-based coupled-cluster methods.

Method	MnH	CrH	CoH	FeH
ROCCSD	153.11	191.66	233.71	241.54
ROCCSD(T)	148.47	191.36	245.52	251.76
ROCCSDT	151.98	191.36	245.17	247.59